Confirmation of the Reality of the Viscoelastic Solutionlike−Meltlike Transition via Optical Probe Diffusion

Kiril A. Streletzky and George D. J. Phillies*

Department of Physics, Worcester Polytechnic Institute, Worcester, Massachusetts 01609

Received July 22, 1998

ABSTRACT: Light scattering spectroscopy was used to study the diffusion of mesoscopic optical probe particles through concentrated aqueous solutions of high molecular weight hydroxypropylcellulose. Optical probe spectra in solutions of this polymer are bimodal, consisting of fast and slow modes. Hydroxypropylcellulose solutions show an apparent viscoelastic solutionlike−meltlike transition, at which the concentration dependence of the solution viscosity η changes from a low-concentration stretched exponential form to a high-concentration power-law form. We studied the influence of this apparent viscoelastic transition on the optical probe spectrum $S(q,t)$. The concentration dependence of the fast mode has a sharp change near the solutionlike−meltlike transition concentration c^+. The slow mode fitting exhibits smaller changes near c^+ in its concentration dependence. It has been suggested that solutionlike−meltlike transition seen in the viscosity measurements is only an artifact of the curve-fitting procedures used to analyze that data. Our results here on an independent physical quantity, namely $S(q,t)$, confirm the physical reality of the solutionlike−meltlike transition.

Introduction

Creation of a model describing adequately polymer dynamics in nondilute solutions is a major quest of macromolecular science. Several extant models treat polymer transport properties quite differently.[1−9] Numerous experimental studies[10−20] have tested these models by measuring the polymer self-diffusion coefficient D_s, polymer viscosity η, and other variables for a wide range of polymer concentrations c, molecular weights M, and solvent quality conditions. Literature reviews[5,21,22] of experimental phenomenology identify empirical laws for D_s and η over a wide range of concentrations, from highly dilute to very concentrated, including concentrations considerably higher than the nominal overlap concentration c^*. These empirical laws for D_s and η have[5,21] the form of stretched exponentials, namely

$$D_s = D_0 \exp(-ac^{\nu}M^{\gamma}) \tag{1}$$

and

$$\eta = \eta_0 \exp(a'c^{\nu'}M^{\gamma'}) \tag{2}$$

Here a and a' are scaling prefactors, and ν, ν', γ, and γ' are scaling exponents. At the same time, it is well-known that the power laws $D_s \sim M^{-2}$ and $\eta \sim M^{3,4}$ describe adequately the experimental findings for polymer melts.

An important implication of this coexistence of two different molecular-weight dependences for D_s or η is the existence of a transition between these forms at some concentration c^+. The molecular-weight dependence of η changes at the concentration c^+ from a stretched-exponential behavior in M in semidilute solutions ("solutionlike" behavior) to a power-law in M behavior in concentrated solutions or melts ("meltlike" behavior). If eqs 1 and 2 fail with increasing c at fixed M, then not only the M but also the c-dependence of eqs 1 and 2 must fail at some concentration c^+. A recent literature review[21] and experimental studies by Phillies et al.[10,11] indeed find a transition in η from the stretched-exponential ("solutionlike") behavior at $c < c^+$

$$\eta = \eta_0 \exp(\alpha c^{\nu}) \tag{3}$$

to the power-law ("meltlike") behavior at $c > c^+$

$$\eta = \bar{\eta}c^{x} \tag{4}$$

in some but not all systems.

A change in the molecular weight dependence of the polymer self-diffusion coefficient D_s can also be reasonably expected at some concentration. However, in most cases considered previously in ref 21, D_s follows eq 1 for all concentrations studied, including concentrations at which η has power-law behavior.

The polymer chosen for this study—1MDa hydroxypropylcellulose (HPC)—is an uncharged, semirigid, water-soluble polymer. This polymer has a relatively low solutionlike−meltlike transition c^+, seen experimentally in the very detailed viscosity study of Phillies et al.[10] Reference 10 found that $\eta(c)$ of 1MDa HPC has a sharp solutionlike−meltlike transition at $c^+ = 6$ g/L and $\eta \approx 144$ cP. Specifically, at $c < c^+$ η follows eq 3 with $\eta_0 = 0.85$, $\alpha = 0.97$, and $\nu = 0.93$; at $c > c^+$, η follows eq 4 with $x = 4.33$. Reference 10 demonstrated that $\eta(c)$ is continuous and analytic through the transition; i.e., $\eta(c)$ and $\partial(\log(\eta(c)))/\partial(\log(c))$ are both continuous at c^+. Because 1MDa HPC has a very low c^+, which makes sample preparation procedures and the conventional light scattering experiment much easier, HPC is an ideal system for studying the effect of solutionlike−meltlike transition on polymer transport properties.

Phillies and Quinlan[10] interpreted their measurements as showing a lower-concentration stretched-exponential regime, a higher-concentration power-law regime, and a sharp transition at c^+. However, this interpretation is not unique. In particular, one could

* To whom communication may be addressed. E-mail: phillies@wpi.wpi.edu.

10.1021/ma981156a CCC: $18.00
Published on Web 12/17/1998

alternatively interpret the low-concentration regime as a series of power-law regimes separated by broad crossover regions, the final crossover region ending at c^+. In this alternative interpretation, the stretched exponential behavior is merely a numerical approximant lacking fundamental meaning, and nothing of great physical interest happens at c^+. The primary objective of this paper is to determine which of these two alternatives is correct by applying an additional physical technique, namely optical probe diffusion, to study the HPC−water system.

This paper also extends our earlier study of optical probe diffusion in this system[23] to higher concentrations. The earlier paper confined itself to the solutionlike regime $c < c^+$, while in this paper we extend measurements well into the meltlike regime $c > c^+$.

This paper is based on a use of the optical probe diffusion technique. A typical optical probe diffusion experiment (pioneered by Turner and Hallett[24]) uses quasielastic light scattering spectroscopy (QELSS) to monitor the motion of highly scattering mesoscopic probe particles (for example, polystyrene latex spheres) through a practically unseen polymer matrix, inferring information about polymer dynamics. In an optical probe diffusion experiment, if the spectral line shape is an exponential, then the diffusion coefficient D_p of the probes can be easily calculated from the initial slope of the spectrum. However, in the case of highly nonexponential spectra, D_p calculated from the initial slope does not resolve between short- and long-time behavior.

Several earlier probe diffusion studies in HPC[11,15,26] have revealed that the spectra of probes diffusing in 1MDa HPC are highly bimodal, implying a need for detailed spectral analysis. Using a systematic analysis of the spectral line shape, this laboratory recently found[23] an adequate functional form for describing these bimodal spectra and studied systematically[23,27] the physical properties of the spectral modes in the solutionlike regime ($0 \le c \le 7$ g/L). This paper extends our analysis to probe diffusion experiments in the meltlike regime ($c > 7$ g/L). The objective is to search for an influence of the solutionlike−meltlike transition on the optical probe spectrum.

The next section describes our experimental equipment and spectral fitting techniques. Further sections describe our results and data interpretation. A discussion closes the paper.

Experimental Methods

The polymer studied in this work was hydroxypropylcellulose (HPC), nominal molecular weight 1 MDa (Scientific Polymer Products). Stock solutions of HPC−water with concentration of 15 g/L were prepared with water purified by Millipore Milli-RO and Milli-Q systems (purified water resistivity was 14−18 MΩ/cm). Solutions of lower concentrations (0−15 g/L) were prepared by serial dilution of the stock solution. A trace (0.2 wt %) of surfactant (TX-100 (Aldrich)) was added to the stock solution to prevent HPC absorption by the probe particles. The surfactant concentration was chosen following the control experiments of Phillies et al.[11]

Carboxylate-modified polystyrene latex spheres (PSL) of nominal diameters 50, 87, and 189 nm (Interfacial Dynamics) were used as optical probes. In a probe diffusion experiment, it is important to make sure that the observed light scattering spectrum corresponds to scattering by probes moving through a practically unseen polymer matrix. Because latex spheres are very good scatterers, even trace amounts of PSL (1−5 μL per mL of polymer solution) were found to be enough for probes to dominate the scattering intensity. In order to avoid probe multiple scattering, we kept probe volume fractions under 0.001.

We performed several control experiments to test if there is any noticeable contribution to the scattered light from the concentration fluctuations of the polymer. We compared under identical operating conditions the scattering intensity of probe-free polymer solutions with the scattering intensity of the same polymer solutions after addition of optical probes. Typically, the scattering by the probe-free polymer solutions was less than 1% of the probe−polymer scattering. Relaxational modes corresponding to the diffusion of surfactant, micelles, and polymer chains scatter too little light to be seen under our experimental conditions. Therefore, our spectra correspond with a high accuracy to the motion of optical probes through the invisible polymer solution. One can also directly subtract the probe-free polymer spectrum from the probe−polymer spectrum and then analyze the difference spectrum, comparing it with the probe−polymer spectra. In an earlier paper[23] we performed these subtraction tests for spectra of probes that are much smaller (with $d = 14$ nm) than the ones used in this study. Reference 23 found that at all c (up to 7 g/L), the line shape of the difference spectrum has exactly the same functional form as the probe−polymer spectrum. However in this study there is no need to make such tests in systematic way, because probes here are much larger and scatter much more light than 14 nm spheres. In fact probes scatter more than 99% of the total probe−polymer scattering. In contrast, scattering of 14 nm probes in 7 g/L of HPC contributed just 96% to the total scattering.

Solutions were clarified by passing them through cellulose filters (Micron Separations) with pore diameters of 1.2 μm into glass fluorimeter cuvettes (NSG Precision Cells, Inc) with four sides polished. Even though this pore size is much larger than any of the probes in this study, we had to use this pore size to limit the filtration time to 45−60 min, because HPC solutions of high concentration (7−15 g/L) are very viscous. However, our initial solvent is very clean; the aforementioned control experiments comparing probe−polymer−solvent and polymer−solvent spectra confirm that this filter pore diameter is adequate to exclude dust from our samples.

The sample cells were placed into a decalin-filled index-matching vat inside a copper assembly, maintained at 25 ± 0.1 °C by a Neslab RTE-110 water circulator and temperature regulator. Cells were illuminated by a Spectra-Physics 2020−03 Ar^+ CW laser with a maximum power output of 2W at $\lambda = 514.5$ nm. Scattered light was detected by a BI-200SM photometer-goniometer (Brookhaven Instruments). We used a 270-channel Brookhaven Instruments BI2030AT digital multitau correlator to analyze the spectra.

Here we studied HPC solutions in the concentration range $7 < c \le 15$ g/L using latex spheres of diameters 50, 87, and 189 nm. Each sample was subject to at least three measurements under identical experimental conditions (same laser power, optical geometry, correlator sample time, integration time, etc.) to guarantee the reliability of the data. We also performed a few control experiments on low-concentration ($0 \le c \le 7$ g/L) samples prepared from our 15 g/L stock solution, in order to test the reproducibility of the data at low c relative to our previous paper. We found good agreement between these spectra on samples diluted from the 15 g/L stock solution and results of ref 23. Most light scattering experiments were conducted at a scattering angle $\theta = 90°$. However, we also studied the q-dependence of $S(q,\tau)$ for 87 and 189 nm probes at concentrations of 8, 10, 12, and 15 g/L of HPC. Our angular experiments covered the range of internal scattering angles $34° \le \theta \le 107°$ with typical steps between measurements of 5−10°.

In quasielastic light scattering spectroscopy (QELSS) one studies the temporal evolution of fluctuations in the scattered intensity $I(q,t)$ by calculating the intensity−intensity correlation function:

$$S(q,\tau) = \int_0^T \mathrm{d}t\, I(q,t)I(q,t+\tau) \qquad (5)$$

Here τ is a shift in time, T is the duration of the experiment, and q is the magnitude of the scattering vector.

The intensity−intensity correlation function $g^{(2)}(q,t)$ is related to the field-correlation function $g^{(1)}(q,t)$ via

$$g^{(2)}(q,t) = S(q,t) - B = A(g^{(1)}(q,t))^2 \quad (6)$$

where A is the scattering amplitude and B is the baseline (the time-independent part of the spectrum). We analyzed spectra by fitting a field correlation function $g^{(1)}(q,t)$ to specific functional forms, rather than by fitting $g^{(1)}(q,t)$ to a generic form such as Koppel's cumulant expansion.[28] Cumulant analysis works well for dilute polydisperse systems[28] but fails to represent separately the short and the long time relaxations of the spectra observed in our experiments. We tried several forms for $g^{(1)}(q,t)$, and using nonlinear least-squares methods and the simplex algorithm,[29] we minimized $[g_f^{(2)}(q,t) - g_e^{(2)}(q,t)]^2/[g_e^{(2)}(q,t)]^2$, where $g_f^{(2)}$ and $g_e^{(2)}$ are fitted and experimentally measured forms of intensity−intensity correlation function, respectively. In our fitting procedure, we varied initial values of fitting parameters to see if the output of the fit depended on the initial value of the fitting parameters. The fit was considered unstable if upon changing the initial guesses for fitting parameters the outcome of the fit changed by more than 1−2%.

Results

Analyzing the spectra of probes in 1MDa HPC we found that $g^{(1)}(t)$ is bimodal, namely

$$g^{(1)}(q,t) = A_f \exp(-\theta_f t^{\beta_f}) + (1 - A_f) \exp(-\theta t^{\beta}) \quad (7)$$

Here θ and θ_f are the relaxation pseudorates of the slow and fast modes, β and β_f are the stretching exponents of the slow and fast modes, and A_f is the amplitude fraction of the fast mode. For probe sizes studied here (50, 87, 189 nm), we found that $\beta \approx 1$, but keeping β as a free parameter produced considerably less stable and reproducible fits than forcing $\beta = 1$. This instability with β as a free parameter is caused by overparametarization of the fits, which introduces an excessive compliance of the fitting function, thereby increasing the scatter in the fitting parameters without obtaining an improvement in the rms error.

We measured light scattering spectra $S(q,t)$ with high accuracy by using the multitau option of the correlator combined with a splicing procedure. The multitau option divides the correlator channels into banks of adjacent channels, each bank having a different sample time, so that the channel spacing can be greater at long delay times than is needed at short delay times. Our splicing fitting procedure consisted of simultaneously fitting eq 7 to a series of three or four spectra of the same sample, each spectrum having a different sample time δt, sample times of each spectrum being spaced by a factor of 8−9 from the previous spectrum. To extend the range of time scales covered by each spectrum and to reduce the number of spectra to be spliced to a minimum, we used the multi-τ option for the shorter sample time spectra; for each solution, the longest-sample-time spectrum of sample was run with a constant sample time to cover long relaxation times with a high density of data points. For the smallest δt, we used a sample time of 1 μs to ensure good representation of short time scales. For the longest δt, we used a sample time which allowed the correlator to cover the complete decay of the spectrum. All spectra for each solution sample were fit (on the level of the intensity correlation function) to one functional form with a single set of fitting parameters, and a separate amplitude A for each spectrum. For spectra with small δt the correlation function does not decay to the true baseline; for these spectra we used the baseline data points as additional data channels.

This splicing technique has been used before, e.g. by Carroll and Patterson[30] and by Phillies and Lacroix;[31] however, these authors did not combine multi-τ spectra into their splicing procedure. Using our splicing technique with multitau spectra enabled us to cover 5−7 decades in time and a 100−1000-fold decay of $g^{(2)}(q,t)/g^{(2)}(q,0)$. This range is very important because our polymer solutions had relaxation times as long as few seconds and as short as few microseconds.

The very slow process of probe diffusion through a concentrated polymer solution requires very long integration times. For our long-sample-time experiments we used integration times of 5−10 h. For our most concentrated samples we ran long-sample-time experiments for 25 h.

The spectral line shape (eq 7) that we found to describe probe relaxation in $c > 7$ g/L 1MDa HPC is consistent with findings of ref 23 for intermediate and large probe particles, as defined in that paper, these being probes with diameter $d \approx R_h$ and $d > R_g$, respectively. Here R_h is the polymer hydrodynamic radius and R_g is the polymer radius of gyration. Probes used here (d = 50, 87, 189 nm) are in the intermediate and large probe ranges. The functional form of $g^{(1)}(t)$ is the same at all polymer concentrations. Both at $c \leq 7$ g/L and at $7 < c \leq 15$ g/L, the sum of a fast stretched exponential and slow pure exponential (eq 7) describes $g^{(1)}(t)$ adequately.

Concentration Dependence of the Optical Probe Spectra

This section describes the concentration dependences of the fitting parameters θ, θ_f, β_f, and A_f from eq 7 for large and intermediate probes over the concentration range $0 \leq c \leq 15$ g/L. (The exponent β is a constant and has no concentration dependence.) Data for $0 \leq c \leq 7$ g/L is primarily from ref 23; higher concentration results are new here. We first discuss the fitting parameters that show the most radical change in their concentration dependence at the solutionlike−meltlike transition. We then consider the behavior of the other fitting parameters.

Figure 1 shows the concentration dependence of the fast relaxation pseudorate θ_f for intermediate and large probes of 50, 87, and 189 nm. Reference 23 found that θ_f is independent of concentration at $c \leq 7$ g/L for all probes studied ($14 \leq d \leq 455$ nm). For 87 and 189 nm probes, we here find at $c > 7$ g/L the appearance of a very strong concentration dependence of θ_f. For these probes, θ_f falls 20−100-fold as c increases from 7 to 15 g/L. The transition in the concentration dependence of θ_f happens near 6−7 g/L. This transition concentration is very close to the solutionlike−meltlike transition c^+ of 6 g/L that was determined[10] from the concentration dependence of η. For the intermediate-size 50 nm probes, there is only a very small change of c dependence of θ near c^+; at $c \geq 6$ g/L, θ_f decreases only weakly as c rises. However, 50 nm probes are close to the small−large probe crossover discussed in refs 23 and 27, and for $c < c^+$ small probes were previously shown[23] to behave very differently from large probes.

How does θ_f depend on c for $c > c^+$? As seen in Figure 1, for all probes at $c \geq c^+$, $\log(\theta_f)$ is approximately linear

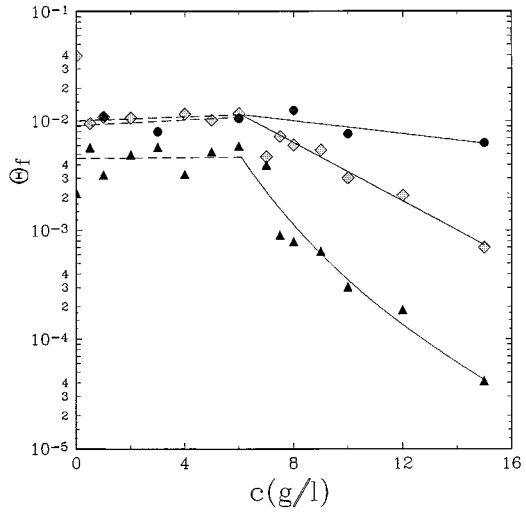

Figure 1. Concentration dependence of the fast relaxation pseudorate θ_f (eq 7) for probes of diameter 50 (●), 87 (◇), and 189 (▲) nm. Most data for $c \leq 7$ g/L are from ref 23. For $c \leq 6$ g/L, dashed lines are pure exponentials in c. Solid lines for $c > 6$ g/L are as follows: (1) pure exponentials in c for 50 and 87 nm probes; (2) power law in c for 189 nm probes. Fitting parameters are given in Table 1. In 1MDa HPC, c^+ is at 6 g/L. Units of θ_f are $(\mu S)^{-\beta_f}$.

Table 1. Concentration Dependence of θ_f, Parametrized as $\theta_f = \theta_{f0} \exp(-\alpha c^\nu)$ (Function A) at Low c and as $\theta_f = \theta_{f0} \exp(-\alpha c^\nu)$ (Function A) or as $\theta_f = \theta_{f0} c^\nu$ (Function B) at High c (θ_f from Eq 7)

d (nm)	c (g/L)	function	θ_{f0}	α	ν	RMS error
50	≤6	A	9.78×10^{-3}	-6.98×10^{-4}	1.0	0.25
	≥6	A	1.74×10^{-2}	-6.86×10^{-2}	1.0	0.19
87	≤6	A	1.01×10^{-2}	-2.14×10^{-2}	1.0	0.056
	≥6	A	7.45×10^{-2}	0.31	1.0	0.094
		B	3.15		−3.02	0.20
189	≤6	A	5.01×10^{-3}	-1.88×10^{-3}	1.0	0.22
	≥6	A	0.136	0.55	1.0	0.37
		B	5.80		−5.22	0.38

in c, suggesting the use of a pure exponential as a fitting function. Solid lines for 50 and 87 nm probes represent the fits of θ_f to a pure exponential. (The pure exponential fit for 189 nm probes is not shown.) The fitting parameters are given in Table 1. It is difficult to determine accurately the transition concentration between the c-independent and the c-dependent regimes, because near $c = 5-7$ g/L, θ_f is somewhat scattered. The choice of transition concentration affects the parameters for the exponents (Table 1). A crossover at 6 g/L seems reasonable to us, but we do not claim uniqueness for this choice. We also fit θ_f at $c \geq 6$ g/L to a power law $\theta_f = \theta_{f0} c^\nu$. Parameters from this fit appear in Table 1. For 50 and 87 nm probes, the power law fit is worse than the exponential fit. For 189 nm probes, the power law fit works as well as the pure exponential fit. As an example, Figure 1 shows the power law fit for 189 nm probes at $c > 6$ g/L. From Figure 1, θ_f is generally smaller for larger probes. At c^+ there is a quantitative change in the d dependence of θ_f: The decrease in θ_f with increasing d is considerably more pronounced at $c > 6$ g/L than at $c < 6$ g/L.

Figure 2 shows the concentration dependence of the fast mode stretching exponent β_f for intermediate and large probes. There is again a radical change in the concentration dependence of β_f near 5−7 g/L. For all spheres, at $c \leq 7$ g/L, β_f falls linearly with increasing c.

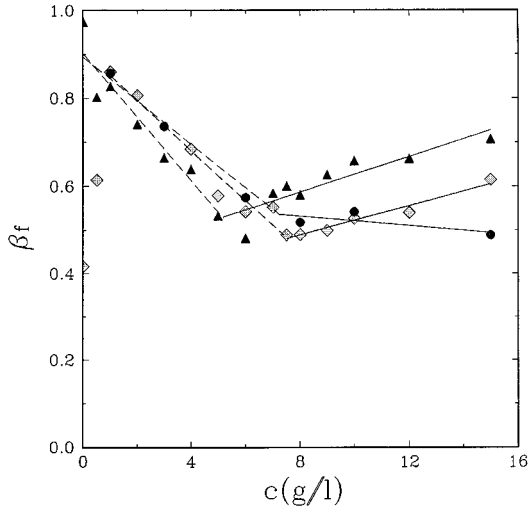

Figure 2. Stretching exponent β_f of the fast relaxation (eq 7) as a function of HPC concentration for probes of diameter 50 (●), 87 (◇), and 189 (▲) nm. Lines are linear fits to data at low c (dashed lines) and high c (solid lines).

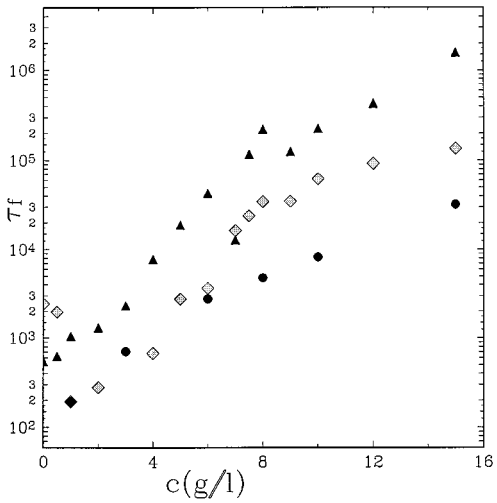

Figure 3. Concentration dependence of the relaxation time $\tau_f = \theta_f^{-1/\beta_f}$ for probes of diameter 50 (●), 87 (◇), and 189 (▲) nm. θ_f and β_f are from eq 7.

Above the transition concentration, β_f increases linearly with increasing c (87 and 89 nm probes) or is nearly independent of concentration (50 nm probes). For all three probes, the visible change in the concentration dependence of β_f is seen approximately at the solutionlike−meltlike transition concentration c^+ of 6 g/L.

Note the qualitative change in the d dependence of β_f at c^+. At $c < c^+$, β_f of larger probes is generally smaller than β_f of smaller probes. At $c > c^+$, the relation between smaller and larger probe β_f is inverted: β_f of 189 nm probes always larger than β_f of 50 or 87 nm probes.

Figure 3 presents concentration dependence of the relaxation time $\tau_f = \theta_f^{-1/\beta_f}$. τ_f increases with rising c over the whole concentration range $0 \leq c \leq 15$ g/L. However, for 87 and 189 nm probes the rate of increase of log τ_f with increasing c is smaller above 7 g/L than below 7 g/L. Over the range $0 \leq c \leq 7$ g/L, τ_f increases by more than 2 orders of magnitude with increasing c, while over the range $7 \leq c \leq 15$ g/L τ_f increases by less than 1 order of magnitude. The concentration dependence of the fast mode relaxation time is definitely weaker in the meltlike regime than it is in the solutionlike regime.

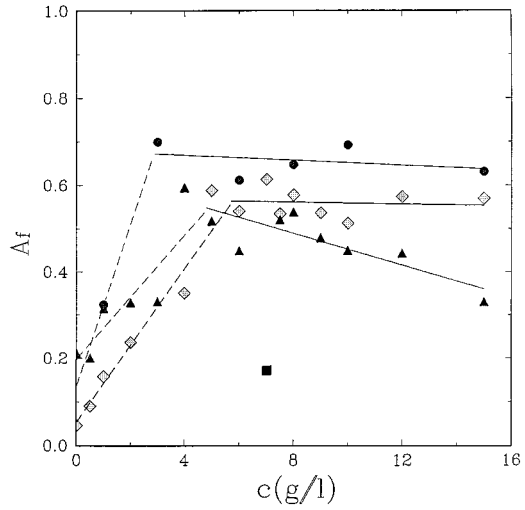

Figure 4. Amplitude fraction parameter A_f of the fast relaxation (eq 7) as a function of HPC concentration for 50 (●), 87 (◇), and 189 (▲) nm probes. Lines are linear fits to data at low c (dashed lines) and high c (solid lines). Points (■) are omitted from the fit.

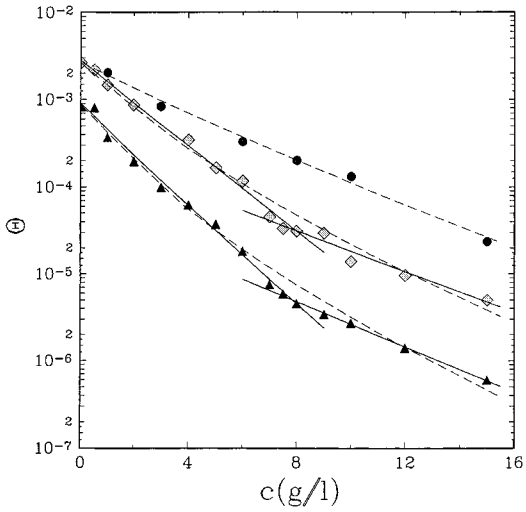

Figure 5. Concentration dependence of the slow relaxation pseudorate θ (eq 7) for probes of diameter 50 (●), 87 (◇), and 189 (▲) nm. Dashed lines are stretched exponentials in c, fit to the whole concentration range $0 \le c \le 15$ g/L. Solid lines are stretched exponentials in c, fit separately to low and high concentrations. Fitting parameters are given in Table 2.

Figure 4 gives the concentration dependence of the fast mode fraction parameter A_f. Even though the data is considerably scattered near c^+, for 87 and 189 nm probes the general trend is clear: A_f increases with increasing c until it reaches a plateau at $c \approx 4-6$ g/L; with further increases of c, A_f does not change for the 87 nm probes, and decreases somewhat for the 189 nm probes. For 50 nm probes, above 4 g/L A_f is largely concentration independent.

Figure 5 gives the concentration dependence of the slow relaxation pseudorate θ. In contrast to Figures 1−3, there is no sharp change in the concentration dependence of θ near c^+. For all spheres, θ decreases monotonically with increasing c. However, for 87 and 189 nm probes, the rate of decrease of $\log(\theta)$ with increasing c is smaller at $c > 7$ g/L than at $c < 7$ g/L; θ decreases more than 100-fold as c increases from 0 to 7 g/L, but decreases only 10-fold as c increases from 7 to 15 g/L. Above the solutionlike−meltlike transition the concentration dependence of θ weakens. For 50 nm probes, there is no visible change in the c dependence of θ at c^+.

Table 2. Concentration Dependence of θ, Parametrized as $\theta = \theta \exp(-\alpha c^\nu)$ (Function C) over All c and as $\theta = \theta \exp(-\alpha c^\nu)$ (Function A) at Low c and as $\theta = \theta \exp(-\alpha c^\nu)$ (Function A) or as $\theta = \theta c^\nu$ (Function B) at High c (θ from eq 7)

d (nm)	c (g/L)	function	θ_0	α	ν	RMS error
50	all c	C	2.82×10^{-3}	0.40	0.91	0.11
87	$c \le 7.5$	A	2.81×10^{-3}	0.56	1.0	0.13
	$c \ge 7.5$	A	3.42×10^{-4}	0.35	0.93	0.15
		B	1.29×10^{-2}		−2.90	0.17
87	all c	C	3.71×10^{-3}	0.72	0.97	0.25
189	$c \le 7.5$	A	9.19×10^{-4}	0.71	0.97	0.15
	$c \ge 7.5$	A	1.23×10^{-4}	0.63	0.79	0.038
		B	4.00×10^{-3}		−3.23	0.088
189	all c	C	1.49×10^{-3}	1.33	0.67	0.25

We fit θ to several different functional forms using a nonlinear least-squares algorithm. We tried one stretched exponential at all c, two stretched exponentials (one at low and one at high c), and a stretched exponential at low c followed by a power law at high c. Table 2 summarizes our findings. The fit of θ to a single stretched exponential $\theta_0 \exp(-\alpha c^\nu)$ over the whole concentration range (Figure 5, dashed lines) works well only for 50 nm probes. For 87 and 189 nm probes, there is a systematic deviation of θ from a single stretched exponential at intermediate concentrations $7 \le c \le 10$ g/L. This visible break in the c dependence of θ near c^+ encouraged us to fit θ to two separate stretched exponentials. Fits of θ to one stretched exponential at low c and to another stretched exponential at high c (Figure 5, solid lines) have a much smaller rms error than does the fit to a single stretched exponential. As a crossover concentration between exponentials, we chose 7.5 g/L. The choice of crossover concentration has a modest effect on the exponential parameters. With our choice of crossover concentration, the fitting parameters for the low-c exponential are within experimental error the same as the fitting parameters found by ref 23. We also tried to fit θ at $c \ge 6-8$ g/L to power laws in c. For 87 and 189 nm probes, power-law fits are always slightly worse than stretched exponential fits. Fits to a power law are not shown in Figure 5, but typical fitting parameters appear in Table 2. We do not claim we have found a unique functional form describing θ for $c > c^+$, however, we demonstrated a change in c-dependence of θ near c^+.

Finally, consider the d -dependence of θ. From Figure 5, θ decreases with increasing d. In the concentration range $0 \le c \le 7.5$ g/L, the decrease in θ with increasing d is larger at higher concentrations: θ of 50 nm probes is larger than θ of 189 nm probes by a factor of 3 at 0 g/L and by a factor of 60 at 7.5 g/L. However, in the range $7.5 \le c \le 15$ g/L the d dependence of $d\theta/dc$ disappears: θ of 50 nm and θ of 189 nm probes have the same ratio at 7.5 and at 15 g/L.

In conclusion, of the four concentration-dependent fitting parameters (θ, θ_f, β_f, and A_f) that describe our spectra, at least two (θ_f and β_f), which characterize the fast mode, show a radical change in their concentration dependence near the solutionlike−meltlike transition concentration c^+. A third fitting parameter, the pseudorate θ of the slow relaxation, also changes its c dependence near c^+, though not as radically as θ_f or β_f.

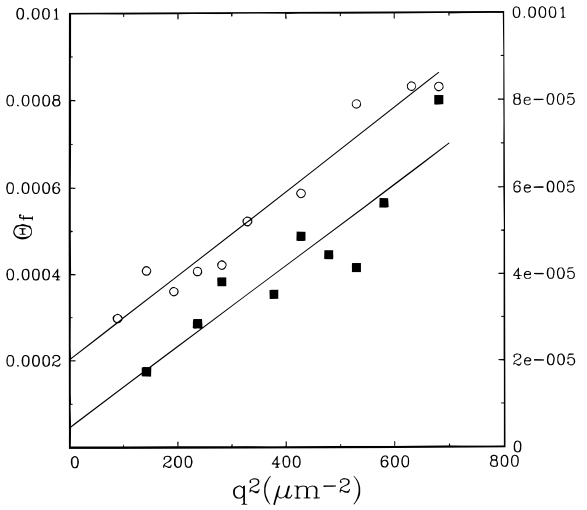

Figure 6. Fast decay pseudorate θ_f (eq 7) as a function of q^2 for 189 nm probes in 8 (○) and 15 (■) g/L of HPC−water. Left vertical scale is for 8 g/L data. Right vertical scale is for 15 g/L data. Solid lines are fits linear in q^2.

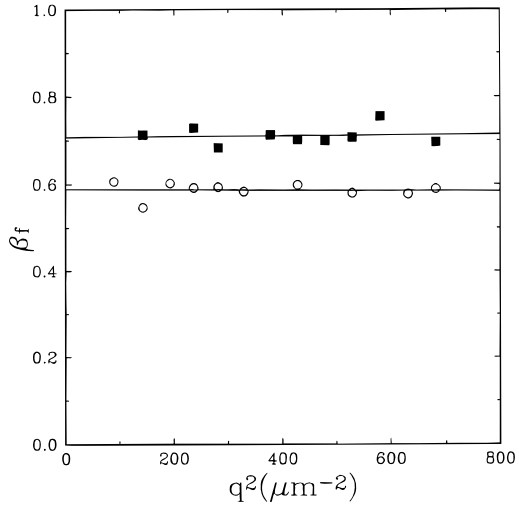

Figure 7. Stretching exponent β_f (eq 7) as a function of q^2 for 189 nm probes in 8 (○) and 15 (■) g/L of HPC−water. Solid lines are fits linear in q^2.

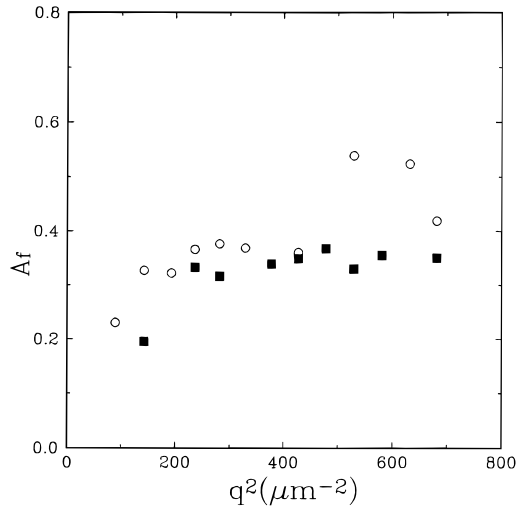

Figure 8. Amplitude fraction parameter A_f (eq 7) as a function of q^2 for 189 nm probes in 8 (○) and 15 (■) g/L of HPC−water.

The relaxation time $\tau_f = \theta_f^{-1/\beta_f}$ of the fast mode also changes its concentration dependence near c^+. Finally, the fraction parameter A_f changes its c-dependence at a concentration below c^+, near $c \approx 4$ g/L.

Angular Dependence of the Optical Probe Spectra

Reference 23 addressed the angular dependence of spectra of large spheres at $c < 7$ g/L, finding the q dependences of the fast and slow modes to be very different. At $c < 7$ g/L the pseudorate θ shows[23] a clear diffusive behavior with $\theta \sim aq^2$. The stretching exponent β_f was found to be q-independent at $c < 7$ g/L. The fractional amplitude A_f was found[23] to increase weakly with increasing q at low angles ($q^2 < 300\ \mu m^{-2}$) but to be q independent at high angles ($q^2 > 300\ \mu m^{-2}$). Finally, at $c < 7$ g/L, the pseudorate θ_f has[23] a very complicated q dependence, being q independent at some wave vectors, but linear in q^2 with a nonzero intercept b at other wave vectors.

Here we examine the q dependences of the fitting parameters at $c > 7$ g/L. Figures 6−9 give typical q-dependences of the fitting parameters for 189 nm probes at 8 and 15 g/L. The angular behaviors of fitting parameters seen here are representative of data at all four concentrations (8, 10, 12, and 15 g/L) and both sphere sizes (87 and 189 nm) for which the q dependence of the spectrum was studied.

Figure 6 gives exemplary q dependences of θ_f at 8 and 15 g/L of HPC for 189 nm probes. As noted above, θ_f depends strongly on c. θ_f increases with increasing q^2. To within the scatter in the data there is a linear dependence $\theta_f \sim aq^2 + b$ with a large intercept b. Comparing Figure 5 with ref 23, there is no profound change in the q dependence of θ_f between the solution-like and the meltlike regimes, even though the c dependence of θ_f changes dramatically at c^+.

Figure 7 shows β_f as a function of q^2 for 189 nm probes at 8 and 15 g/L of HPC. β_f is generally independent of q^2. The q dependences seen in Figure 6 are the same as q dependences reported in ref 23 at $c < 7$ g/L for the same probes.

Figure 8 shows A_f as a function of q^2 for 189 nm probes at 8 and 15 g/L of HPC. A_f increases slightly over the observed range of q. Comparing our results with ref 23, over $0 \le c \le 15$ g/L there are few changes in the q dependence of A_f. At $c < 7$ g/L, for 189 nm probes A_f increases[23] with rising q at low q but is q independent at high q. However, at $c > 7$ g/L, one can not easily identify two different regions of q-behavior for 189 probes, perhaps because above 7 g/L the data are slightly more scattered than data with $c < 7$ g/L.

Figure 9 shows exemplary q dependences of θ at 8 and 15 g/L for 189 nm probes. As noted in the previous section, θ depends strongly on HPC concentration. θ shows clear diffusive behavior with $\theta \sim aq^2$ and a very small (if any) intercept as $q^2 \rightarrow 0$. This q dependence of θ is the same as the q dependence seen at $c < 7$ g/L[23] for these spheres.

In summary, the parameters we use to describe $g^{(1)}(q,t)$ either are independent of q (e.g., β_f), depend weakly on q (e.g., A_f), or are approximately linear in q^2 (e.g., θ, θ_f). In the linear response regime, hydrodynamic transport coefficients are expected to be linear in q^2. The observed q^2 dependence of θ and approximate q^2 dependence of θ_f constitute strong evidence that θ and θ_f are proper linear transport coefficients.

The previous section concluded that θ_f, β_f, A_f, and θ all change their concentration dependences near the

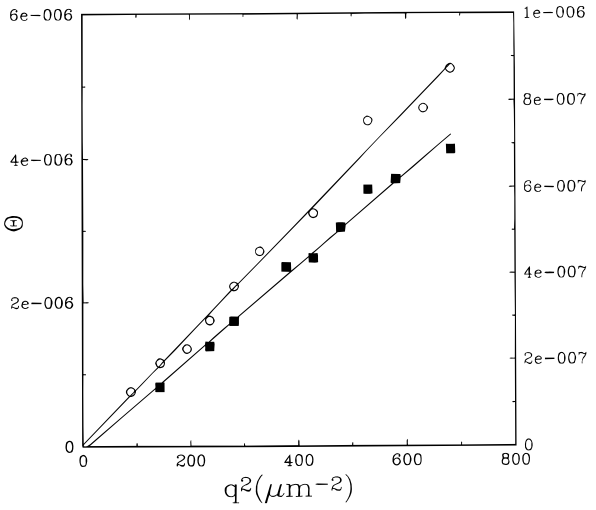

Figure 9. Slow relaxation pseudorate θ (eq 7) as a function of q^2 for 189 nm probes in 8 (○) and 15 (■) g/L of HPC−water. Left vertical scale is for 8 g/L data. Right vertical scale is for 15 g/L data. Solid lines are fits linear in q^2.

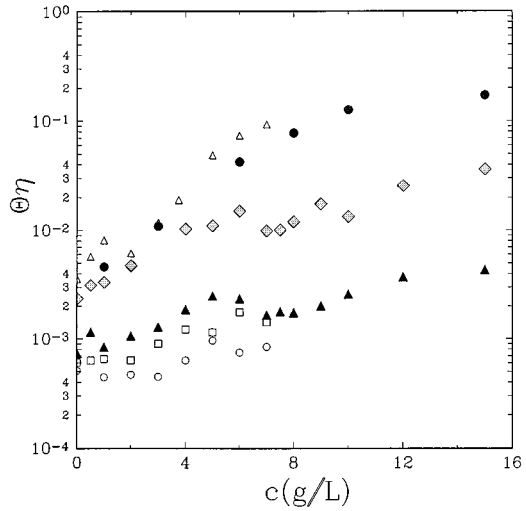

Figure 10. Concentration dependence of $\theta\eta$ for intermediate probes of diameter 50 (●), 67 (△), and 87 (◇) nm and for large probes of diameter 189 (▲), 282 (□), and 455 (○) nm. η is from ref 10. Most data for $c \leq 7$ g/L are from ref 23.

viscosity solutionlike−meltlike transition concentration c^+. These conclusions referred to measurements taken with a 90° scattering angle. From the results of this section, if the analysis of the previous section on the c dependence had used data taken at some other scattering angle, it would have reached precisely the same conclusions.

Relationships between the Viscosity and Spectral Parameters

We now compare the concentration dependences of θ and θ_f with the concentration dependence of the zero-shear viscosity η, as obtained earlier by Phillies and Quinlan.[10] θ and θ_f for $c \leq 7$ g/L include results from ref 23, except for the 50 nm probe data, which were taken in this study.

Figures 10 and 11 give the concentration dependences of $\theta\eta$ and $\theta_f\eta$, respectively. Consider first Figure 10. For large probes (189, 282, and 455 nm) at $c \leq 7$ g/L, $\theta\eta$ is almost constant, fluctuating within 2−3-fold of its average value. For 189 nm probes at $c > 7g/L$, θ tracks η^{-1} to within a factor of 2 of its average value. Over the whole range $0 \leq c \leq 15$ g/L, $\theta\eta$ increases only by a factor of 4−5. For intermediate 87 nm probes, $\theta\eta$ increases by a factor of 5 as c increases from 0 to 7 g/L; over $7 \leq c \leq 15$ g/L, $\theta\eta$ increases by a further factor of 3. Finally, for the intermediate 50 nm probes $\theta\eta$ increases by a factor of 20 over the range $0 \leq c \leq 7$ g/L but only by a factor of 2−3 over the range $7 < c \leq 15$ g/L.

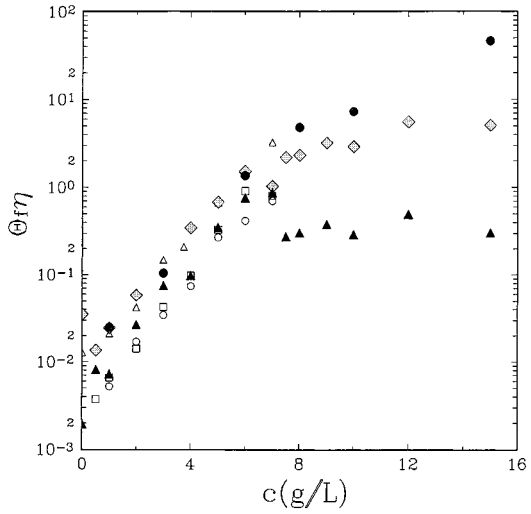

Figure 11. Concentration dependence of $\theta_f\eta$ for intermediate probes of diameter 50 (●), 67 (△), and 87 (◇) nm and for large probes of diameter 189 (▲), 282 (□), and 455 (○) nm. η is from ref 10. Most data for $c \leq 7$ g/L are from ref 23.

Consider now the behavior of θ_f (Figure 11). For 87 and 189 nm probes, near 7 g/L there is a radical change in the concentration dependence of $\theta_f\eta$. Over the range $0 \leq c \leq 7$ g/L, $\theta_f\eta$ of any of our probes increases by a factor of 100 with rising c. However, over the range $7 \leq c \leq 15$ g/L, $\theta_f\eta$ of the 189 nm probes is independent of concentration, $\theta_f\eta$ of the 87 nm probes increases only by a factor of 5, and $\theta_f\eta$ of the 50 nm probes increases with rising c only by a factor of 10. The change in the c-dependence of $\theta_f\eta$ at the solutionlike−meltlike transition concentration c^+ is very marked, because θ_f changes its c dependence dramatically at c^+, and at the same concentration, η changes its c-dependence from a stretched exponential to a power law in c. Because $\theta_f\eta \approx$ const for 189 nm probes for $c > c^+$, in this concentration regime the concentration dependence of θ_f should be largely the same as the concentration dependence of η^{-1}, namely a power law. Indeed, our data for $\theta_f(c)$, particularly for 189 nm probes, can be successfully fit by a power law (e.g., Figure 1 and Table 1). However, the fitting exponents differ somewhat with $x = 4.33$ for $\eta(c) = \bar{\eta}c^x$ and with $\nu = 5.22$ for $\theta_f = \theta_{f0}c^{-\nu}$.

In summary, in the solutionlike regime $c < c^+$ the fast mode pseudorate θ_f of intermediate and large probes does not follow the concentration dependence of η^{-1}. $\theta_f\eta$ increases by approximately 2 orders of magnitude over the solutionlike regime. However, in the meltlike regime, θ_f suddenly becomes sensitive to the concentration dependence of the macroscopic solution viscosity, so that $\theta_f\eta$ is nearly independent of c for $c > c^+$. The relation between the slow mode pseudorate θ and η does not dramatically change at c^+. For large 189 nm probes, $\theta(c)$ tracks $\eta^{-1}(c)$ to similar extents in the solutionlike and meltlike regimes. For intermediate 50 and 87 nm probes, $\theta(c)$ follows $\eta^{-1}(c)$ better for $c > c^+$ than for $c < c^+$. For intermediate probes, a radical change in the c dependence of $\theta_f\eta$ and a small change in the c-dependence of $\theta\eta$ are seen to occur near c^+. For large probes,

a radical change in c dependence of $\theta_f\eta$ is seen near c^+. The solutionlike−meltlike transition seen by ref 10 in $\eta(c)$ and reported here in θ_f, β_f, and θ is also visible in the c dependences of $\theta_f\eta$ and $\theta\eta$.

Discussion

Here we studied probe diffusion of intermediate and large probes in the meltlike concentration regime of 1MDa HPC. Our previous study[23] addressed probe diffusion of the same spheres in the solutionlike concentration regime. The solutionlike and meltlike regimes are defined by the concentration dependence of the viscosity; at the transition concentration c^+, the concentration dependence of η changes from the stretched exponential behavior of eq 3 to the power law behavior of eq 4. For our polymer, the transition concentration is [10] $c^+ \approx 6$ g/L.

Both below and above c^+, light scattering spectra of large ($d \geq R_g$) and intermediate ($R_h \leq d \leq R_g$) probes are bimodal, as expressed by eq 7. How does the transition in the concentration dependence of η affect the behavior of the two independent modes in our probe spectra?

At c^+, the fast-mode parameters θ_f and β_f radically change their concentration dependences. The concentration dependences of the relaxation time $\tau_f = \theta_f^{-1/\beta_f}$ and $\theta_f\eta$ also change markedly at c^+. While there are dramatic changes at c^+ in the concentration dependence of the fast mode parameters, the q dependences of the parameters remain the same above and below c^+.

The slow mode parameters θ, β, and $1 - A_f$ show similar behavior above and below c^+. At c^+, θ values for 87 and 189 nm probes slightly change their concentration dependences. However, the change in $\theta(c)$ at c^+ is not strong. Both above and below c^+, $\theta(c)$ has approximately a stretched exponential concentration dependence with modestly different fitting parameters. There is also small change in the concentration dependence of $\theta\eta$. For 50 and 87 nm probes, $\theta(c)$ follows $\eta^{-1}(c)$ slightly better for $c > c^+$ than for $c < c^+$. Finally, above c^+ the slow mode retains the diffusive behavior ($\theta \sim aq^2$) that it has below c^+.

In conclusion, this paper studied the effect of the solutionlike−meltlike transition on optical probe spectra. Near the concentration c^+, where the solution viscosity η changes its concentration dependence,[10] we find radical changes in the behavior of the fast mode spectral parameters and slight changes in the behavior of the slow mode spectral parameters. The observed changes near c^+ in the behavior of the optical probe spectra $S(q,t)$ confirm the conclusion of Phillies et al.[10] that the solutionlike−meltlike transition is a real physical effect and not an illusion created by a hypothesized flexibility of the stretched exponential as a fitting function.

Acknowledgment. The partial support of this work by the National Science Foundation under Grant DMR94-23702 is gratefully acknowledged.

References and Notes

(1) de Gennes, P.-G. *J. Chem. Phys.* **1971**, *55*, 572.
(2) de Gennes, P. G. *Scaling Concepts in Polymer Physics*; Cornell University Press: Ithaca: NY, 1979.
(3) Doi, M.; Edwards, S. F. *The Theory of Polymer Dynamics*; Oxford University Press: Oxford, England, 1986.
(4) Phillies, G. D. J. *Macromolecules* **1995**, *28*, 8198.
(5) Phillies, G. D. J. *J. Phys. Chem.* **1989**, *93*, 5029.
(6) Tsang K.-Y.; Ngai, K. L. *Phys. Rev. E* **1997**, *54*, R3067.
(7) Tsang K.-Y.; Ngai, K. L. *Phys. Rev. E* **1997**, *56*, R17.
(8) Ngai, K. L.; Phillies, G. D. J. *J. Chem. Phys.* **1996**, *105*, 8385.
(9) Ngai, K. L.; Rendell, R. W. Philos. Mag. B **1998**, *77*, 621.
(10) Phillies, G. D. J.; Quinlan, C. *Macromolecules* **1995**, *28*, 160.
(11) Phillies, G. D. J.; Richardson, C.; Quinlan, C. A.; Ren, S.-Z. *Macromolecules* **1993**, *26*, 6849.
(12) Lin, T.-H.; Phillies, G. D. J. *J. Colloid Interface Sci.* **1984**, *100*, 82.
(13) Lin, T.-H.; Phillies, G. D. J. *J. Phys. Chem.* **1982**, *86*, 4073. Lin, T.−H.; Phillies, G. D. J. *Macromolecules* **1984**, *17*, 1686.
(14) Ullmann, G. S.; Phillies, G. D. J. *Macromolecules* **1983**, *16*, 1947. Ullmann, K.; Ullmann, G. S.; Phillies, G. D. J. *J. Colloid Interface Sci.* **1985**, *105*, 315.
(15) Brown, W.; Zhou, P. *Macromolecules* **1989**, *22*, 4031. Zhou, P.; Brown, W. *Macromolecules* **1989**, *22*, 890. Phillies, G. D. J.; Brown, W.; Zhou P. *Macromolecules* **1992**, *25*, 4948.
(16) Wheeler, L. M.; Lodge, T. P. *Macromolecules* **1989**, *22*, 3399. Won, J.; Onyenemezu, C.; Miller, W. G.; Lodge, T. P. *Macromolecules* **1994**, *27*, 7389. Wheeler L. M.; Lodge, T. P. *Macromolecules* **1986**, *19*, 2983.
(17) Nystrom, B.; Roots, J.; Carlsson, A.; Lindman B. *Polymer* **1992**, *33*, 2875. Nystrom, B.; Walderhaug, H.; Hansen, F. K. *J. Phys. Chem.* **1993**, *97*, 7743.
(18) Mustafa, M. B.; Russo, P. S. *J. Colloid Interface Sci.* **1989**, *129*, 240. Mustafa, M. B.; Tipton, D. L.; Barkley, M. D.; Russo, P. S.; Blum, F. D. *Macromolecules* **1993**, *26*, 370. Russo, P. S.; Mustafa, M.; Cao, T.; Stephens, L. K. *J. Colloid Interface Sci.* **1988**, *122*, 120.
(19) Furukawa, R.; Arauz-Lara, J. L.; Ware, B. R. *Macromolecules* **1991**, *24*, 599.
(20) Yang, T.; Jamieson, A. M. *J. Colloid Interface Sci.* **1988**, *126*, 220.
(21) Phillies, G. D. J. *J. Phys. Chem.* **1992**, *96*, 10061.
(22) Skolnick, J.; Kolinski, A. *Adv. Chem. Phys.* **1990**, *78*, 223.
(23) Streletzky, K. A.; Phillies, G. D. J. *J. Chem. Phys.* **1998**, *108*, 2975.
(24) Turner, D. N.; Hallett, F. R. *Biochem. Biophys. A.* **1976**, *451*, 305.
(25) Brown, W.; Rymden, R. *Macromolecules* **1986**, *19*, 2942.
(26) Bu, Z.; Russo, P. S. *Macromolecules* **1994**, *27*, 1187.
(27) Streletzky, K. A.; Phillies, G. D. J. *J. Polym. Sci. B: Polym. Phys.*, in press.
(28) Koppel, D. E. *J. Chem. Phys.* **1972**, *57*, 4814.
(29) Noggle, J. H. *Physical Chemistry on a Microcomputer*; Little, Brown and Company: Toronto, Canada, 1985.
(30) Carroll, P. J.; Patterson, G. D. *J. Chem. Phys.* **1985**, *82*, 9.
(31) Phillies, G. D. J.; Lacroix, M. *J. Phys. Chem. B* **1997**, *101*, 39.

MA981156A